Nanocrystallisation of rare tolbutamide form V in mesoporous MCM-41 silica

Karol P. Nartowski[a,b], Diksha Malhotra[a], Lucy E. Hawarden[a,c], László Fábián[a] and Yaroslav Z. Khimyak[a]*

[a]School of Pharmacy, University of East Anglia, Norwich Research Park (UK)

E-mail:Y.Khimyak@uea.ac.uk

[b]Department of Drug Form Technology, Faculty of Pharmacy, Wroclaw Medical University, ul. Borowska 211, 50-556 Wroclaw (Poland).

[c]Drug Product Science and Technology, Bristol-Myers Squibb, Reeds Lane, Moreton, Merseyside, CH46 1QW (UK)

Encapsualtion of pharmaceuticals inside nanoporous materials is of increasing interest due to their possible applications as new generation therapeutics, thernostic platforms or smart devices. Mesoporous silicas are leading materials to be used as nanohosts for pharmacueticals. Further development of new generation of nanoscale therapeutics requires complete understanding of the complex host–guest interactions of organic molecules confined in nanosized chambers at different length scales. In this context we present results showing control over formation and phase transition of nanosize crystals of model flexible pharmaceutical molecule tolbutamide confined inside 3.2 nm pores of the MCM-41 host. Using low loading levels (up to 30 wt. %) we were able to stabilise the drug in highly dynamic amorphous/disordered state or direct the crystallisation of

1

the drug into highly metastable nanocrystalline form V of tolbutamide (at loading levels of 40 and 50 wt. %), providing first experimental evidence for crystallisation of pharmaceuticals inside the pores as narrow as 3.2 nm.

Introduction

Mesoporous silicas have attracted much interest in materials science due to unique features including synthetically controllable architecture of the pores and pore size diameter, large surface area and possible functionalisation of the silanol groups on the materials surface.[1-5] Recently, mesoporous silica nanoparticles have gained increasing importance for pharmaceutical applications as intracellular drug delivery systems or novel diagnostic platforms.[1,6-12] Controllable encapsulation and manipulation of the drug phase under nanoscale confinement make these materials interesting as nanoscale crystallisation chambers for polymorph screening, leading to discoveries of new crystalline phases or stabilization of metastable crystals.[13,14] For example Ward and co-workers demonstrated formation of new polymorphs of pimelic acid, suberic acid and coumarin when confined inside CPG material (controlled pore glass) with pore sizes lower than 23 nm.[13,15] Selective crystallisation and stabilisation of metastable form of paracetamol (form III) was demonstrated by Beiner and co-workers inside the CPG with pore size (d) in the range from 22 nm to 103 nm and stabilisation of amorphous drugs inside smaller pores (below 10 nm).[16,17]

The investigation of structure and phase transitions of confined nanosize crystals using PXRD and DSC is far from trivial, due to a decrease of long range ordering in the materials, reflected in broadening of the PXRD peaks and decrease and broadening of the melting peak of confined crystals.[15,17,18] Furthermore, simultaneous presence of molecules in different physical states and motional regimes inside the mesopores makes detailed characterisation of such complex

composites very challenging.[18-20] Therefore, application of methods sensitive to the local environment of atoms (namely solid-state NMR) is of high importance for molecular-level understanding of crystallisation and phase transitions of pharmaceuticals.[21-24]

Recently we have demonstrated controllable crystallisation and stabilisation of metastable indomethacine form V inside the 30 nm pores of MCF material (Mesoporous Cellular Foam).[18] Furthermore, we developed a ^{19}F MAS NMR protocol to probe the local environment of confined flufenamic acid in situ and showed for the first time the simultaneous presence of confined molecules as nanocrystalline, amorphous and highly mobile species adsorbed at the silica surface during confined crystallisation.[21] A recent study of Navrotsky and co-workers demonstrated crystallisation of the iodide salt of the rigid, spherical organic ion N,N,N-trimethyl-1-adamantammonium (TMAAI, 321,3 g mol^{-1}) within 12.8 nm pores of SBA-15 type silica and the coexistence of crystalline and amorphous species inside the pores using ^{13}C MAS NMR and selectively labelled (^{13}C) TMAAI.[25] Furthermore, the authors indicated that a pore size of at least one unit cell and temperature below the (depressed) melting point can serve as sufficient indicators of the formation of confined nanocrystals.[25] This is in agreement with the crystallisation of ibuprofen (206.3 g mol^{-1}) confined within 11.6 nm pores of SBA-15 at 223 K reported by Azais et al.[26]

Based on our previous findings[18,21] and the recent report from Navrotsky's group[25], we have selected a small and flexible molecule (tolbutamide, 270.35 g mol^{-1}) as a model to probe hypothesis that size and flexibility of organic molecules, together with high loading levels within the pores play an essential role in the successful crystallisation of pharmaceuticals inside porous hosts even with relatively narrow mesopores. Tolbutamide (TB) contains a rigid benzene ring and a highly mobile aliphatic chain with seven bonds that can rotate freely. The high flexibility of this structure

has led to a large number of TB polymorphs reported in the Cambridge Structural Database (7 structures including a high Z' form III).[27–32] Due to its high flexibility, TB adopts different conformations in different crystal forms making it a representative example of conformational polymorphism.[27] Furthermore, due to its low glass transition temperature (Tg = 277 K) and crystallisation during cooling of the molten drug it is a challenging material to be stabilised in its amorphous state.[33–36] Using several complementary techniques (N_2 adsorption, PXRD, DSC and solid-state NMR), we have demonstrated that TB can be encapsulated within the pores of MCM-41 silica host with relatively narrow mesopores (diameter ca. 3.2 nm, much smaller than that for SBA-15, MCF or CPG silicas) using melt loading method. Through the gradual increase of the guest content we have achieved gradual filling of the pores and showed that the model drug can be successfully stabilised in it amorphous state at drug loadings up to 30 wt% or its crystallisation can be directed into metastable form V as confirmed using PXRD and solid-state NMR corroborated by DFT calculations. As previously reported by Nath et al., TB form V could only be obtained using crystallisation from acidified methanol and it is stable for only few hours at room temperature.[29] In this work we demonstrate for the first time crystallisation of metastable TB form V inside the pores of MCM-41 (3.2 nm) silica scaffold and also report in-situ monitoring of its phase transition to TB form I[H] using solid-state NMR.

Experimental Section

Materials and Synthetic protocols

Materials

Tolbutamide, n-hexadecyltrimethylammonium bromide, ammonia, ethanol, tetraethyl orthosilicate (TEOS), methanol were all purchased from Sigma-Aldrich.

Synthesis of MCM-41

Spherical, homogenous MCM-41 particles were synthesised according to the method previously published by Grün et al.[37] In a typical synthesis, 2.5 g of n-hexadecyltrimethylammonium was dissolved in miliQ quality water (50 mL). A solution of ammonia (37% wt., 13.2 g) and ethanol (60 g) was mixed with the already prepared n-hexadecyltrimethylammonium solution. The solution was stirred for 15 minutes and 4.7 g of TEOS was added, resulting in a mixture of the following composition: 1 TEOS: 0.3 C_{16}TMABr: 11 NH_3: 144 H_2O: 58 EtOH. After stirring for 2 hours, a precipitate was formed, filtered and washed using methanol and deionized water. The material was dried at 363 K overnight and calcined at 823 K for 5 hours.

Drug loading

TB (guest) was loaded into MCM-41 (host) using the melt loading method. Briefly, the drug and the host were mixed in a glass vial for 3 minutes using a spatula in host:guest ratios of 85:15, 80:20, 75:25, 70:30, 60:40 and 50:50 (wt/wt). The obtained mixture of the powders was heated on a hot plate at 408 K, i.e. above the melting point of TB, and mixed with spatula for 5 minutes, ensuring that the drug can be adsorbed within the pores via capillary action. Once loaded, the samples were cooled to room temperature and stored within a desiccator.

Characterisation methods

Differential scanning calorimetry (DSC)

DSC analysis was carried out using a Q2000 MTDSC instrument (TA Instruments, New Castle, DE, US). Crimped aluminium pans were used for all analyses. The sample weights ranged from 2-4 mg for pure crystalline samples, and 8-10 mg for loaded drug:silica composites. A nitrogen

flow rate of 50 mL/min was used. The sample was heated with a heating rate of 5 K/min from 253 to 408 K followed by cooling with 20 K/min to 253 K and subsequent heating with a heating rate of 5 K/min to 408 K. The data were analysed using the TA Instruments Universal Analysis 2000 software (TA Instruments-Waters LLC).

Thermogravimetric analysis (TGA)

A TQ500 thermogravimetric analyser (TA Instruments, New Castle, DE, US) was used to determine the drug content within the composites. The samples (weight 5-10 mg) were heated at a rate of 5 K/minute from 298 K to 373 K to determine content of water adsorbed within the material and then further with heating rate of 30 K/minute to 873 K. The sample was kept at 873 K for 15 minutes to ensure complete decomposition of the drug and then heated to 903 K. The samples were then cooled to room temperature. The analysis was performed in an inert gas atmosphere with 50 mL/min purge of N_2. TA Instruments Universal Analysis 2000 software (TA Instruments-Waters LLC) was used to analyse the data.

Powder x-ray diffraction (PXRD)

ARL TM X'TRA Powder Diffractometer (Thermo Fisher Scientific Inc., Waltham, MA, US) was used with Cu Kα radiation with a wavelength of 0.15424 nm. The composites were analysed in the angular range 2θ from 6-36° and the step size of 0.01° using scanning rate of 6 seconds per step. The analysis was performed at room temperature.

Scanning electron microscopy (SEM)

The SEM images of the synthesized material were taken using a JSM 4900 LV microscope (JEOL Ltd, Japan) at 20 kV. Prior to the analysis the samples were sputtered with thin film of gold.

Nitrogen adsorption-desorption analysis

Nitrogen adsorption-desorption isotherms were measured using a Nova 2200e Surface Area and Pore Size Analyzer (Quantachrome, Hook, UK) at 77 K. All samples were outgassed under a high vacuum at 313 K for 12 h prior to the analysis to avoid any temperature driven recrystallization of the loaded drug. The BET specific surface area was calculated over a relative pressure range from 0.05 to 0.20 assuming monolayer coverage and a molecular area of the nitrogen of 0.162 nm^2. The pore size distribution curves were calculated by applying the NLDFT method implemented in the NovaWin (ver. 11.03) software (Quantachrome Instruments) using spherical/cylindrical pore model and N_2 adsorption on silica at 77 K.

Nuclear magnetic resonance spectroscopy (NMR)

All solid-state NMR spectra were acquired using a Bruker AVANCE III solid-state NMR spectrometer with a Larmor frequency of 400.23 MHz for ^1H and 100.64 MHz for ^{13}C. ^1H-^{13}C cross-polarisation/magic angle spinning experiments (CP/MAS) were acquired using the RAMP CP pulse sequence. The MAS spinning rate was 10.0 kHz, the ^1H $\pi/2$ pulse length was optimised to 3.20 μs along with optimisation of the pulse delay to 10.0 s. SPINAL64 decoupling was used and the contact time (for CP) was set to 2.0 ms. The number of scans changed from 1024 for crystalline phases and high loading composites (30-50%) to 6144 for materials loaded with TB at concentration of 15-25 %. TMS was used as a reference. ^1H NMR spectra were acquired using 16 scans and single $\pi/2$ pulse sequence without decoupling. The variable temperature (VT) experiments were performed in the temperature range from 293 to 373 K in 10 K steps. The temperature of the sample was stabilised for 5 min before spectra acquisition. The temperature

control was achieved using a Bruker BCU II chilling unit and a standard heater implemented in the probe.

^{1}H Solution-state NMR spectra of TB were recorded using Bruker Avance I spectrometer equipped with a triple resonance probe operating at 499.69 MHz for [1]H. The obtained spectra corroborated by online spectra predictor[38] and CASTEP calculations were used for ^{1}H assignment.

^{1}H and ^{13}C NMR chemical shift calculations using first principles. Computations were performed using the CASTEP code.[39] Geometry optimisation was carried out with constrained cell parameters and positions of all heavy atoms using the PBE exchange-correlation functional[40] with the addition of the Tkatchenko and Scheffler (TS) model[41], a plane wave basis set cut-off energy of 1100 eV and ultrasoft pseudopotentials[42].

The NMR chemical shieldings were calculated using the gauge including projector augmented wave approach (GIPAW)[43] and a cut-off energy of 1100 eV. The isotropic NMR shieldings computed with CASTEP were converted to chemical shifts using the following equation:

$$\delta_{calc} = \sigma_{ref} - \sigma_{iso},$$

where σ_{iso} is the isotropic chemical shielding generated from first-principles calculations and $\sigma_{ref} = 169.5$ ppm (for ^{13}C) and 30.6 ppm (for ^{1}H) as reported by Bradley et al.[44]

Results and discussion

Effect of drug loading on the mesoscopic parameters of MCM-41 host
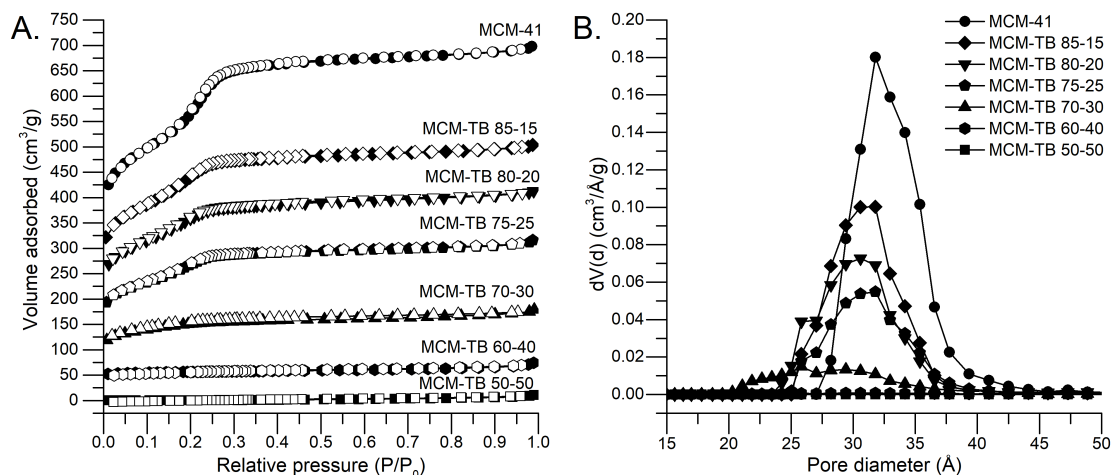

Figure 1. Nitrogen adsorption/desorption isotherms (left) and pore size distribution (right) of MCM-41 host and TB loaded composites. The isotherms are offset by 50 cm³/g. The adsorption step is presented in black and desorption step is presented in white points in the isotherms.

Table 1. Drug content and structural parameters of MCM-41 host and loaded composites.

Host-guest composite	TB (g/g)	V_{total} [cm³/g]	d_{pore} [Å]	S_{BET} [m²/g]
MCM-41	N/A	0.66	32	1277
MCM-TB 85-15	0.163	0.39	32	780
MCM-TB 80-20	0.211	0.33	31	614
MCM-TB 75-25	0.254	0.26	31	485
MCM-TB 70-30	0.317	0.12	28	176
MCM-TB 60-40	0.420	0.05	N/A	35
MCM-TB 50-50	0.504	0.02	N/A	2

Synthesised submicrometer spherical particles of MCM-41 host with pore size diameter of ca. 3.2 nm were loaded with tolbutamide using the melting method. Loaded composites analysed with nitrogen adsorption/desorption isotherms show a gradual decrease of the total pore volume and surface area with increasing drug content (Figure 1, Table 1). These results are corroborated by low angle PXRD, where gradual attenuation of the d[100] reflections is observed with increasing drug content (Figure 2). This may be attributed to a reduction in the X-ray scattering contrast between the silica walls and the pore filling material and not to a loss of crystallinity of the MCM-41 host.[45] Thermogravimetric analysis of the drug-SiO_2 composites confirmed that the expected drug content was achieved during loading and loading temperature was below the thermal degradation point of the drug (see ESI Figure S2). It is important to mention that water content of final composites was low and ca. 1-2 wt. % as determined by TGA.
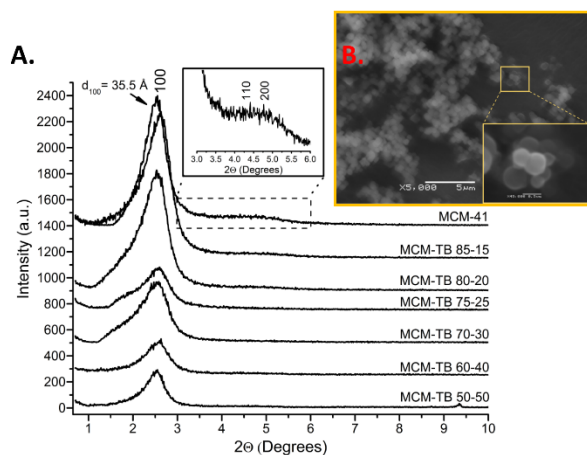

Figure 2. A. Low angle PXRD patterns of MCM-TB composites at different loading levels. B. SEM micrograph of MCM-41 particles.

Formation of confined metastable form V of TB

Amorphous tolbutamide has low glass transition temperature (Tg = 277 K) and is included in the first class of glass forming agents based on the classification system implemented by Taylor et al.[35] Compounds in this class recrystallise during cooling from the undercooled melt state, regardless of cooling rate.[35,36] Based on the results reported by Kawakami et al.[36], supercooled TB recrystallises to form IV on cooling, with a further recrystallisation to form III observed during subsequent heating.

Figure 3. A. PXRD patterns of MCM-TB composites at different drug loadings. The PXRD pattern of TB forms I[L], IV and V were simulated using CSD ref codes: ZZZPUS10[29], ZZZPUS07[27] and ZZZPUS04[46] and B. DSC thermograms of MCM-TB composites and TB form I[L] using the heat-cool-heat cycle.

Tolbutamide encapsulated inside the silica scaffolds using the melting method displayed a very different behavior compared to the bulk drug cooled from the melt. We found that TB remained amorphous at loading levels up to 30 wt. %, with crystallisation into the highly metastable TB form V occurring at higher drug loadings (40-50 wt. %), confirmed using a combination of PXRD, DSC and solid-state NMR. PXRD patterns (Figure 3A) show a broad 'halo' peak due to the

presence of amorphous MCM-TB composites at drug concentrations up to 30 wt. %. The small reflection at d = 8.39 Å observed for composites loaded with TB at 20 and 25 wt. % may indicate the confined guest is present as a mixture of amorphous and partially crystalline TB form V. The synthesized amorphous composites were stable during storage over at least a year. The stabilization of amorphous drug upon confinement in small pores is frequently observed phenomena for highly unstable amorphous pharmaceuticals.[47] The PXRD patterns of the host loaded at 40 and 50 wt. % are in agreement with the simulated PXRD pattern of the highly unstable crystalline TB form V, superimposed on a 'halo' peak of amorphous silica walls and residual amorphous TB confined within the pores.

The observed TB form V has only been formed previously through crystallisation from acidified methanol.[29] The obtained TB form V encapsulated within the mesoporous silica host was stable for at least one month when stored in a desiccator over a silica gel at RT as compared to couple of hours reported by Nath et al.[29] for bulk TB form V (See ESI Figure S5). DSC analysis (Figure 3B) of MCM-TB composites with drug content up to 30 wt. % does not show the melting peaks characteristic of TB polymorphs. The broad endotherm observed here may be related to continuous increase of mobility with increasing temperature and possible transition to liquid-like species for small amount of TB confined within the MCM-41 pores. This phenomenon was previously observed by Navrotsky et al. for confined TMAAl.[25] It can also be related to evaporation of small content of water adsorbed at the surface of the silica. This hypothesis is corroborated by heat/cool/heat DSC cycle data (see ESI Figure S3), which show flattening of the DSC baseline during second heating, after removal of the adsorbed water in the first heating. This phenomenon is frequently observed for drug-silica composites and was discussed by Cordeiro *et al*. for naproxen

confined within MCM-41 and SBA-15 silica hosts.[48] The detailed study of mobility of TB confined in porous silicas will be presented in a separate publication.

At drug loadings of 40 and 50 wt. %, a broad melting endotherm of confined TB form V was observed at 339.9 K followed by recrystallisation and melting of TB form I[H] at 364.2 K. Furthermore, we were able to observe decrease of the glass transition temperature of confined TB in the MCM-TB 50-50 composite (T_g of confined TB = 269 K) during the second DSC heating run indicating differences in mobility of supercooled drug upon confinement as compared to bulk species. Due to the broadening and decrease of the melting point expected with confined crystalline material, TB form I[H] was identified only using variable temperature ^{13}C solid-state NMR spectroscopy (Figure 5). This method enabled us to provide additional information on the supramolecular organisation of tolbutamide in the pores, and to monitor the phase transition of confined drug in situ.

^1H-^{13}C CP/MAS NMR spectra of confined tolbutamide indicate the formation of amorphous drug at low drug content up to 30 wt. % (Figure 4D). The peak broadening is due to the presence of magnetically non-equivalent environments of the carbon atoms alongside increased distribution of possible orientations, typical of amorphous solids. At the higher drug content of 40 and 50 wt. %, much sharper ^{13}C peaks of crystalline TB form V superimposed on broad peaks of residual amorphous TB are observed. This indicates the presence of crystalline TB form V confined within the MCM-41 host, in agreement with PXRD data.
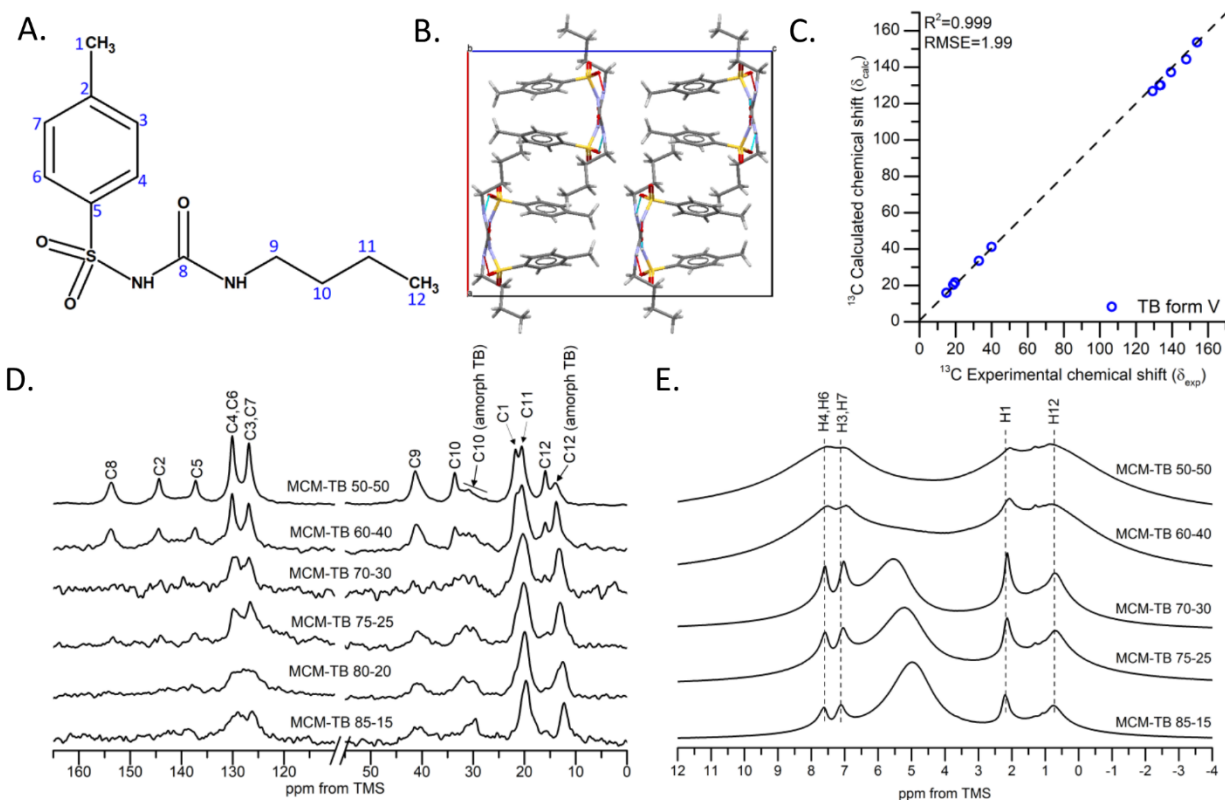
Figure 4. A. TB structure with labelled atoms, B. Packing of TB form V viewed along b axis (CSD ref. ZZZPUS10)[29], C. Experimental ^{13}C chemical shift values for encapsulated TB form V derived from the spectra acquired at 293 K and an MAS rate of 10 kHz vs. calculated ^{13}C chemical shifts using TB form V structure reported by Nath et al. (CSD ref. ZZZPUS10[29]), D. ^{1}H-^{13}C CP/MAS NMR spectra of MCM-TB composites at different drug loadings, E. ^{1}H MAS solid-state NMR spectra of MCM-TB composites at different drug loadings (all spectra acquired at an MAS rate of 10 kHz).

The ^{1}H-^{13}C CP/MAS NMR spectrum of TB form V confined within MCM-41 host is in agreement with the ^{13}C chemical shifts calculated with CASTEP, based on the ZZZPUS10[29] structure reported recently in the CSD.[49] Additionally, a decrease in the peak intensity of the amorphous TB (6144 scans) as compared to crystalline TB (1024 scans) may indicate increased mobility of the confined

amorphous drug, resulting in the inefficient transfer of magnetisation during the cross-polarisation.[50] We recently observed similar phenomenon for flufenamic acid[21] and indomethacin[18] confined within mesoporous silica materials with pore sizes from 3.2 to 30 nm and lactose[51] intercalated within sodium montmorillonite nanocomposites. These findings are in agreement with data presented by Azais et al.[26,52] and Buntkowsky and co-workers.[53] Furthermore, our data are consistent with the results of computational studies of encapsulation of ibuprofen or clotrimazole in MCM-41 silicas postulating the presence of a highly dynamic adsorbed layer of the drug at the surface of the pores.[54,55]

^{1}H MAS NMR spectra of rigid solids usually show very broad peaks due to the presence of strong homonuclear [1]H-^{1}H dipolar interactions. To partially overcome these interactions in ^{1}H solid-state NMR, fast MAS (up to 120 kHz) and/or [1]H-^{1}H homonuclear decoupling sequences are used.[56-58] In the case of confined TB at drug contents up to 30 wt. %, five different proton sites were identified, indicating that the confined drug is in a highly dynamic state. These sites were assigned to the protons of aromatic ring (H4, H7 and H3, H6) and to two CH_3 groups (H1 and H12). The assignment was carried out based on both ^{1}H solution NMR spectra of TB, and CASTEP calculations (see ESI). Further increase of the drug content within the material (40-50 wt. % drug loading) lead to crystallisation of TB inside the pores. This was confirmed by the broadening of the ^{1}H peaks, consistent with the presence of enhanced [1]H-^{1}H dipolar interactions, which are expected for rigid crystalline solids (Figure 4E).

In situ monitoring of phase transitions of TB under confinement via solid-state NMR.

The investigation of phase transitions of confined solids is a considerable analytical challenge due to decrease and broadening of the melting peak in DSC and broadening of PXRD peaks for nano-

size crystals.[13,14,59] In such cases, full understanding of the phase transitions in confinement requires application of methods sensitive to the local environment of atoms, therefore solid-state NMR is ideal to probe both structure and dynamics.
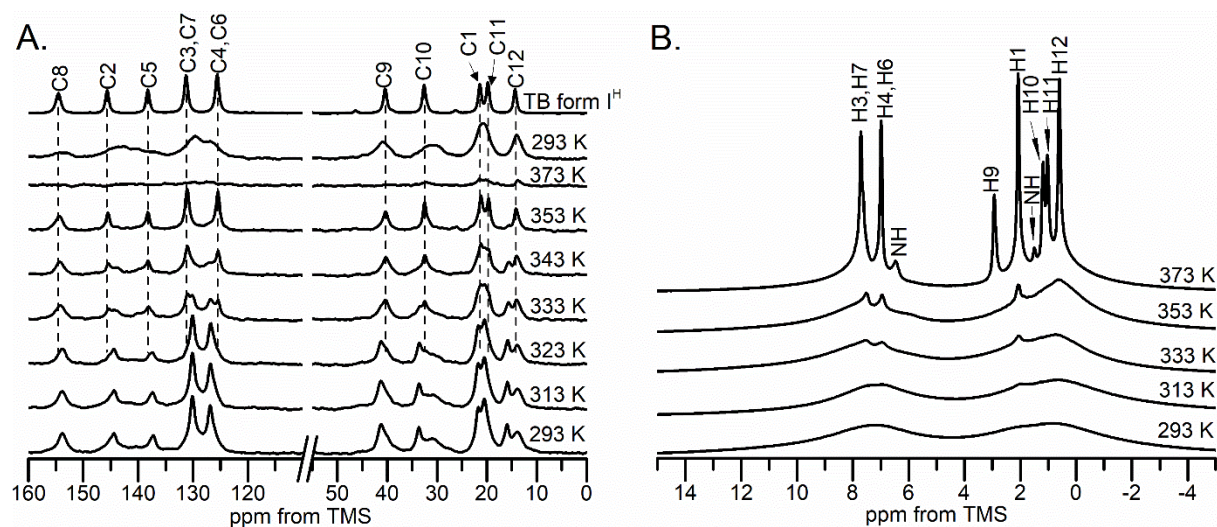

Figure 5 A. ¹H-¹³C CP/MAS B. ¹H MAS solid-state NMR spectra of MCM-TB 50-50 composite and TB form I^H (acquired at 323 K) in the temperature range from 293K to 373K. Peaks are labelled according to the structure in Figure 4A.

At temperatures up to 333 K there was no change observed in the spectra of the MCM-TB 50-50 composite, which is in agreement with DSC analysis. At 333 K peak splitting was detected, which indicated the presence of two crystalline phases. This agrees with DSC results, where the first transition onset was observed at ca. 339 K. With increasing temperature further (up to 343 K) recrystallisation was observed through growth of the peaks associated with form I^H, resulting in only one phase being detected by 353 K, as the confined metastable TB form V underwent a phase transition to TB form I^H. This transition was in agreement with the DSC data, which demonstrated that there is a narrow temperature range at which TB form I^H can be present before it melts at 366 K. When the temperature reached 373 K, the confined drug melted. This was confirmed firstly by

a loss of the CP efficiency observed as a substantial decrease of the peaks intensity in the ^{1}H-^{13}C

CP/MAS spectrum (Figure 5A), and secondly by the significant narrowing of lines in the ^{1}H

spectrum at 373 K, due to an increased mobility (Figure 5B). When the material is cooled to 293

K the ^{1}H-^{13}C CP/MAS NMR spectrum shows broad peaks characteristic of amorphous TB.

The VT ^{1}H MAS spectra of the MCM-TB 50-50 composite with confined TB form V showed a

gradual narrowing of proton peaks H1, H3, H4, H6 and H7 with increasing temperature. The

gradual narrowing of the peaks was attributed to increased dynamics of the aromatic ring of

tolbutamide with increasing temperature. This is not unexpected as all TB polymorphs are

stabilised through the rigid sulfonylurea bonding motif, hence the aromatic ring of tolbutamide

may be in a different motional regime compared to the aliphatic part of the molecule.

Conclusions

We demonstrated that the drug content inside the pores is an important factor in directing formation

of confined nanocrystals for very flexible TB guest species. The model drug TB can be stabilised

in its amorphous state at drug loadings up to 30 wt. % or it can form confined nanocrystals of

metastable form V inside the relatively narrow 3.2 nm mesopores of MCM-41 silica host. Using

VT solid-state NMR spectroscopy, we were able to identify the phase transition from TB form V

to TB form I$^{\text{H}}$, which was difficult to monitor using thermal methods.

ASSOCIATED CONTENT

Supporting Information. Assignment of ^{1}H solid-state NMR spectra of TB based ^{1}H solution-

state NMR experiment and predicted chemical shifts values, heat-cool-heat cycles of DSC

experiments and ^{1}H-^{13}C CP/MAS spectra of MCM-TB 50-50 composite after 10 days and one month of storage are given in ESI.

AUTHOR INFORMATION

Corresponding Author

* Prof. Yaroslav Z Khimyak, School of Pharmacy, University of East Anglia, Norwich Research Park (UK), E-mail:Y.Khimyak@uea.ac.uk

Author Contributions

The manuscript was written through contributions of all authors. All authors have given approval to the final version of the manuscript.

ABBREVIATIONS

TB, tolbutamide, NMR, Nuclear Magnetic Resonance, DSC, Differential Scanning Calorimetry, PXRD, Powder X-Ray Diffraction, TGA, Thermogravimetric Analysis.

REFERENCES

(1)   Giret, S.; Wong Chi Man, M.; Carcel, C. *Chem. - A Eur. J.* **2015**, *21* (40), 13850–13865.

(2)   Vallet-Regí, M.; Ruiz-González, L.; Izquierdo-Barba, I.; González-Calbet, J. M. *J. Mater. Chem.* **2006**, *16* (1), 26–31.

(3)   Linares, N.; Silvestre-Albero, A. M.; Serrano, E.; Silvestre-Albero, J.; García-Martínez, J. *Chem. Soc. Rev. Chem. Soc. Rev* **2014**, *43* (43), 7681–7717.

(4)   Jones, J. T. A.; Wood, C. D.; Dickinson, C.; Khimyak, Y. Z. *Chem. Mater.* **2008**, *20* (10), 3385–3397.

(5)   Hoffmann, F.; Cornelius, M.; Morell, J.; Fröba, M. *Angew. Chem. Int. Ed* **2006**, *45*, 3216–3251.

(6)   Gao, Y.; Chen, Y.; Ji, X.; He, X.; Yin, Q.; Zhang, Z.; Shi, J.; Li, Y. *ACS Nano* **2011**, *5* (12), 9788–9798.

(7)   Vivero-Escoto, J. L.; Slowing, I. I.; Trewyn, B. G.; Lin, V. S.-Y. *Small* **2010**, *6* (18), 1952–1967.

(8)   Xiang, D.; Shigdar, S.; Qiao, G.; Wang, T.; Kouzani, A. Z.; Zhou, S.-F.; Kong, L.; Li, Y.; Pu, C.; Duan, W. *Theranostics* **2015**, *5* (1), 23–42.

(9)   Lee, J. E.; Lee, N.; Kim, T.; Kim, J.; Hyeon, T. *Acc. Chem. Res.* **2011**, *44* (10), 893–902.

(10) Parak, W. J. *Science* **2016**, *351* (6275), 814–815.

(11) Lin, Y.-S.; Tsai, C.-P.; Huang, H.-Y.; Kuo, C.-T.; Hung, Y.; Huang, D.-M.; Chen, Y.-C.; Mou, C.-Y. *Chem. Mater.* **2005**, *17*, 4570–4573.

(12) Juère, E.; Florek, J.; Bouchoucha, M.; Jambhrunkar, S.; Wong, K. Y.; Popat, A.; Kleitz, F. *Mol. Pharm.* **2017**, *14* (12), 4431–4441.

(13) Jiang, Q.; Ward, M. D. *Chem. Soc. Rev.* **2014**, *43* (7), 2066–2079.

(14) Hamilton, B. D.; Ha, J.-M.; Hillmyer, M. A.; Ward, M. D. *Acc. Chem. Res.* **2012**, *45* (3), 414–423.

(15) Ha, J.-M.; Hamilton, B. D.; Hillmyer, M. A.; Ward, M. D. *Cryst. Growth Des.* **2009**, *9* (11), 4766–4777.

(16) Rengarajan, G. T.; Enke, D.; Beiner, M. *Open Phys. Chem. J.* **2007**, *1* (1), 18–24.

(17) Beiner, M.; Rengarajan, G. T.; Pankaj, S.; Enke, D.; Steinhart, M. *Nano Lett.* **2007**, *7* (5), 1381–1385.

(18) Nartowski, K. P.; Tedder, J.; Braun, D. E.; Fábián, L.; Khimyak, Y. Z. *Phys. Chem. Chem. Phys.* **2015**, *17* (38), 24761–24773.

(19) Azaïs, T.; Hartmeyer, G.; Quignard, S.; Laurent, G.; Tourné-Péteilh, C.; Devoisselle, J.-M.; Babonneau, F. *Pure Appl. Chem.* **2009**, *81* (8), 1345–1355.

(20) Skorupska, E.; Jeziorna, A.; Paluch, P.; Potrzebowski, M. J. *Mol. Pharm.* **2014**, *11* (5), 1512–1519.

(21)   Nartowski, K. P.; Malhotra, D.; Hawarden, L. E.; Sibik, J.; Iuga, D.; Zeitler, J. A.; Fábián, L.; Khimyak, Y. Z. *Angew. Chemie Int. Ed.* **2016**, *55* (31), 8904–8908.

(22)   Skorupska, E.; Jeziorna, A.; Kazmierski, S.; Potrzebowski, M. J. *Solid State Nucl. Magn. Reson.* **2014**, *57*, 2–16.

(23)   Dwyer, L. M.; Michaelis, V. K.; O'Mahony, M.; Griffin, R. G.; Myerson, A. S. *CrystEngComm.* **2015**, *33* (4), 395–401.

(24)   Skorupska, E.; Paluch, P.; Jeziorna, A.; Potrzebowski, M. J. *J. Phys. Chem. C* **2015**, *119* (16), 8652–8661.

(25)   Wu, D.; Hwang, S.-J.; Zones, S. I.; Navrotsky, A. *Proc. Natl. Acad. Sci.* **2014**, *111* (5), 1720–1725.

(26)   Azaïs, T.; Tourné-Péteilh, C.; Aussenac, F.; Baccile, N.; Coelho, C.; Devoisselle, J.-M.; Babonneau, F. *Chem. Mater.* **2006**, *18* (26), 6382–6390.

(27)   Thirunahari, S.; Aitipamula, S.; Chow, P. S.; Tan, R. B. H. *J. Pharm. Sci.* **2010**, *99* (7), 2975–2990.

(28)   Kimura, K.; Hirayama, F.; Uekama, K. *J. Pharm. Sci.* **1999**, *88* (4), 385–391.

(29)   Nath, N. K.; Nangia, A. *CrystEngComm* **2011**, *13* (1), 47–51.

(30)   Donaldson, J. D.; Leary, J. R.; Ross, S. D.; Thomas, M. J. K.; Smith, C. H. *Acta Crystallogr. Sect. B Struct. Crystallogr. Cryst. Chem.* **1981**, *37* (12), 2245–2248.

(31)   Drebushchak, T. N.; Pankrushina, N. A.; Boldyreva, E. V. *Dokl. Phys. Chem.* **2011**, *437*

(2), 61–64.

(32)   Drebushchak, T. N.; Drebushchak, V. A.; Pankrushina, N. A.; Boldyreva, E. V. *CrystEngComm* **2016**, *18* (30), 5736–5743.

(33)   Takeuchi, H.; Handa, T.; Kawashima, Y. *Chem. Pharm. Bull. (Tokyo)*. **1987**, *35* (9), 3800–3806.

(34)   Forster, A.; Hempenstall, J.; Rades, T. *J. Pharm. Pharmacol*. **2001**, *53* (3), 303–315.

(35)   Baird, J. A.; Van Eerdenbrugh, B.; Taylor, L. S. *J. Pharm. Sci*. **2010**, *99* (9), 3787–3806.

(36)   Kawakami, K.; Harada, T.; Miura, K.; Yoshihashi, Y.; Yonemochi, E.; Terada, K.; Moriyama, H. *Mol. Pharm*. **2014**, *11* (6), 1835–1843.

(37)   Grün, M.; Unger, K. K.; Matsumoto, A.; Tsutsumi, K. *Microporous Mesoporous Mater*. **1999**, *27* (2–3), 207–216.

(38)   Banfi, D.; Patiny, L. *Chim. Int. J. Chem*. **2008**, *62* (4), 280–281.

(39)   Clark, S. J.; Segall, M. D.; Pickard, C. J.; Hasnip, P. J.; Probert, M. I. J.; Refson, K.; Payne, M. C. *Zeitschrift für Krist*. **2005**, *220* (5/6/2005), 567–570.

(40)   Perdew, J. P.; Burke, K.; Ernzerhof, M. *Phys. Rev. Lett*. **1996**, *77* (18), 3865–3868.

(41)   Tkatchenko, A.; Scheffler, M. *Phys. Rev. Lett*. **2009**, *102* (7), 073005.

(42)   Vanderbilt, D. *Phys. Rev. B* **1990**, *41* (11), 7892–7895.

(43)   Pickard, C. J.; Mauri, F. *Phys. Rev. B* **2001**, *63* (24), 245101.

(44) Bradley, J. P.; Velaga, S. P.; Antzutkin, O. N.; Brown, S. P. *Cryst. Growth Des*. **2011**, *11* (8), 3463–3471.

(45) Gago, S.; Fonseca, I. M.; Parola, A. J. *Microporous Mesoporous Mater*. **2013**, *180*, 40–47.

(46) Donaldson, J. D.; Leary, J. R.; Ross, S. D.; Thomas, M. J. K.; Smith, C. H. *Acta Crystallogr. Sect. B Struct. Crystallogr. Cryst. Chem*. **1981**, *37* (12), 2245–2248.

(47) Rengarajan, G. T.; Enke, D.; Steinhart, M.; Beiner, M.; *J. Mater. Chem*. **2008**, *18* (22), 2537.

(48) Cordeiro, T.; Santos, A. F. M.; Nunes, G.; Cunha, G.; Sotomayor, J. C.; Fonseca, I. M.; Danède, F.; Dias, C. J.; Cardoso, M. M.; Correia, N. T.; Viciosa, M. T.; Dionísio, M. *J. Phys. Chem. C* **2016**, *120* (26), 14390–14401.

(49) Allen, F. H. *Acta Crystallogr. B*. **2002**, *58* (Pt 3 Pt 1), 380–388.

(50) Kolodziejski, W.; Klinowski, J. *Chem. Rev*. **2002**, *102* (3), 613–628.

(51) Hellrup, J.; Holmboe, M.; Nartowski, K. P.; Khimyak, Y. Z.; Mahlin, D. *Langmuir* **2016**, *32* (49), 13214–13225.

(52) Azais, T.; Hartmeyer, G.; Quignard, S.; Laurent, G.; Babonneau, F. *J. Phys. Chem. C* **2010**, *114* (19), 8884–8891.

(53) Buntkowsky, G.; Breitzke, H.; Adamczyk, A.; Roelofs, F.; Emmler, T.; Gedat, E.; Grünberg, B.; Xu, Y.; Limbach, H.-H.; Shenderovich, I.; Vyalikh, A.; Findenegg, G. *Phys. Chem. Chem. Phys*. **2007**, *9* (35), 4843–4853.

(54)   Gignone, A.; Delle Piane, M.; Corno, M.; Ugliengo, P.; Onida, B. *J. Phys. Chem. C* **2015**, *119* (23), 13068–13079.

(55)   Delle Piane, M.; Vaccari, S.; Corno, M.; Ugliengo, P. *J. Phys. Chem. A* **2014**, *118* (31), 5801–5807.

(56)   Sakellariou, D.; Lesage, A.; Hodgkinson, P.; Emsley, L. *Chem. Phys. Lett.* **2000**, *319* (3–4), 253–260.

(57)   Leskes, M.; Madhu, P. K.; Vega, S. *Chem. Phys. Lett.* **2007**, *447* (4–6), 370–374.

(58)   Bielecki, A.; Kolbert, A. C.; Levitt, M. H. *Chem. Phys. Lett.* **1989**, *155* (4–5), 341–346.

(59)   Alcoutlabi, M.; McKenna, G. B. *J. Phys. Condens. Matter* **2005**, *17* (15), R461–R524.

TABLE OF CONTENT

Formation of Tolbutamide form V